ORIGINAL ARTICLE

An Efficient Inclusion Complex Based Fluorescent Sensor for Mercury (II) and its Application in Live-Cell Imaging

Keerthana P[1] · Hanna Abbo[2,3] · Anila Rose Cherian[1] · Salam Titinchi[2] · Anitha Varghese[1]

Abstract

The formation of an inclusion complex between hydroxypropyl-β-cyclodextrin (H-CD) and 4-acetylphenyl-4-(((6-chlorobenzo[d]thiazol-2-yl)-imino)-methyl)-benzoate (L) was investigated by FT-IR, ^{1}H-NMR, X-ray diffraction (XRD), FT-Raman, scanning electron microscope (SEM) techniques in the solid-state, absorption and emission spectroscopy in the liquid state and the virtual state as molecular docking technique. The binding properties of the inclusion complex (H-CD: L) with cations in deionized water was observed via absorbance and photoluminescence (PL) emission spectroscopy. The fluorescence probe (H-CD: L) inclusion complex (IC) was examined for several heavy metal cations, and identified that the PL emission wavelength of the complex displayed a continuous rise in the fluorescence intensity for Hg^{2+}. A linearity range of $1 \times 10^{-8} – 11 \times 10^{-8}$ M and limit of detection value of 2.71×10^{-10} M was found to be achieved for the detection of Hg^{2+}. This outcome proves that the inclusion complex H-CD: L would be a promising material for the development a solid-state fluorescence probe for detecting Hg^{2+}. It also shows application in real sample analysis and cell imaging.

Keywords Hydroxypropyl-beta-cyclodextrin (H-CD) · Inclusion complex · Colorimetric · Hg^{2+} · Fluorescence enhancement · Chemosensor

Introduction

Currently, heavy metal ion pollution is surpassing the threshold limits in various areas of the world due to the growth of industrialization and modernization, for example, coal, and gold mining [1], oil refining [2], and paint production [3]. In comparison to other heavy metal ions, mercury (Hg^{2+}) is the utmost toxic metal pollutant due to its assorted utilisation in numerous industries and horticultural sciences [4, 5]. Non-biodegradable mercury ion prompts extreme tainting of marine resources and soil. Besides, Hg^{2+} gets aggregated in rural and sea-going effluence [6, 7] and causes serious medical and environmental problems, named as myocardial localized necrosis, chemical imbalance, and Minamata sickness [8–11]. As an attempt to ensure human wellbeing, the United States Environmental Protection Agency (USEPA) has proclaimed the Hg^{2+} ion threshold limit value (TLV) in drinking water sources as 2 ppb [12, 13]. In view of, ecological and medical problems related to Hg^{2+}, it is exceptionally fundamental to progress a solid sensing strategy with high sensitivity for observing low levels of Hg^{2+} in the environment and biological systems.

Various analytical techniques like electrochemical methods [14], atomic absorption spectroscopy (AAS) [15], inductively coupled plasma spectroscopy (ICPS) [16], and colorimetry [17] have been used for the detection of various heavy metals. The abovementioned analytical techniques need sophisticated and expensive instruments, tedious preparation, and also pre-treatment of the sample. Among them, the spectrofluorimetric technique has attracted much attention due to its facile and effective method of detecting chemical and biological species, high sensitivity, selectivity, quick response, cost-effectiveness, simplicity and a need of low concentration of analytes [18]. Supramolecular IC has gained more attention compared

✉ Anitha Varghese
  anitha.varghese@christuniversity.in

  Salam Titinchi
  stitinchi@uwc.ac.za

[1] Department of Chemistry, CHRIST (Deemed To Be University), Hosur Road, Bengaluru 560029, India

[2] Department of Chemistry, University of the Western Cape, Cape Town, South Africa

[3] Department of Chemistry, College of Science, University of Basrah, Basrah, Iraq

to other fluorophores like coumarin, pyrene and xanthene derivatives, metallic organic frameworks etc., Supramolecular Inclusion complexes were better and preferable fluorogenic probes for sensing the analytes due to their advantages in selectivity, sensitivity, easy sample preparation, real-time analysis.

Cyclodextrin (CD) belong to the family of cyclic oligosaccharides. It is also known as Schrodinger dextrin's, cycloamyloses and cyclomaltoses. It consists of a macrocyclic ring of glucose subunits joined by α-1,4 glycosidic bonds. Cyclodextrins are obtained from enzymatic hydrolysis of starch. The β-cyclodextrin is a natural oligomer, which has a hydrophobic cavity and an exterior which is highly hydrophilic in nature. The cyclodextrin's hydrophobic interior surface is torus-shaped structure, which permits guest molecules naturally into the hydrophobic cavity by expelling the molecules of water [19]. The cyclodextrins have the ability to form host–guest complex molecule which leads to a number of advantages in different fields [20, 21]. These cyclodextrins (CDs) have been used in number of industries such as pharmaceutical, food, analytical and catalysis. These CDs acts a solubilizers, diluents, tablet ingredients to enhance the solubility, chemical stability, pharma kinetic properties, and bioavailability of drugs [22]. Hydroxypropyl-beta-cyclodextrin (H-CD) is hydrophilic in nature, and considered as a toxic-free derivative at oral and intravenous doses. Recently, H-CD used to increase the stability, solubility and bio-availability of poorly solvable compounds in drug delivery [23].

Acetylphenyl-4-(((6-chlorobenzo[d]thiazol-2-yl)-imino)-methyl)-benzoate (compound L), a crystalline solid is a polycyclic aromatic compound. Compound (L) acts as a fluorescent sensor in a hydrophilic environment. But it exhibits strong fluorescence in the hydrophobic cyclodextrin cavity. It easily binds with mercury metal ions and enhances the fluorescence intensity. In addition, compound (L) has a major role as a fluorescent probe in life cell imaging and real sample analysis. This compound is encapsulated into the H-CD hydrophobic cavity with the release of water molecules.

The key area of the present work is to synthesize H-CD:L solid IC under reflux condition for sensing metal cation. The obtained experimental results showed that the solid IC selectively and sensitively sense mercury metal ion (Hg^{2+}) and it was observed through a visible colour change, absorption and fluorescence spectrum. Based on this phenomenon, a new supramolecular sensor (H-CD: L) has been synthesised by using compound L with H-CD and its more effective in photoluminescence (PL) sensing towards Hg^{2+}. The H-CD: L solid IC shown considerable color variation, PL enhancement upon the addition of Hg^{2+}, which might be used in absorbance and PL sensing for Hg^{2+} in liquid medium. The H-CD: L solid IC could also be applied for real sample analysis and life cell imaging.

Experimental Section

Reagents

Hydroxypropyl-β-cyclodextrin (H-CD) was procured from Sigma Aldrich and used without any further purification. All the chemicals used in this study are of pure analytical grade. Metal chloride salts of Ag^+, Co^{2+}, Cr^{3+}, Cs^+, Hg^{2+}, Ba^{2+}, Mg^{2+}, Fe^{2+}, Fe^{3+}, K^+, Na^+ were obtained from SD Fine-Chem Pvt Ltd., India, metal nitrate salt of Pb^{2+} was obtained from Alfa Aesar, and metal carbonate of Cd^{2+} was obtained from Qualigens and were used without any additional purification. The metal cation solutions (1×10^{-8} M) used throughout the experiment were all prepared in double distilled water.

Apparatus

FT-IR spectrum was used to find out the functional groups and using Thermo Nicolet, Avatar 370. Powder X-ray diffraction (P-XRD) patterns identified from the Rigaku Smart Lab X-ray diffractometer using Cu Kα radiation (λ = 1.5406 Å). Lab RAM HR FT-Raman module, with excitation at 532 nm LASER used to record Raman spectrum. The photophysical studies like the UV–Vis Absorption spectrum were investigated using a Shimadzu UV–visible spectrophotometer (UV–visible 1800). All fluorescence measurements were taken using Shimadzu spectrofluorometer (RF5301PC). All measurements were recorded using PBS buffer solution at pH = 7 medium.

Synthesis of 4-Acetylphenyl 4-(((6-chlorobenzo[d]thiazol-2-yl) imino) methyl) benzoate

Compound (L) was synthesized via two steps reaction: Schiff base synthesis followed by esterification reaction [24].

STEP-1

The Schiff base was synthesized by reacting equimolar quantities (0.01 mol) of 2-amino-6-chlorobenzothiazole and 4-formylbenzoic acid in 40 ml of pure ethanol. Then 3 drops of glacial acetic acid were added continuously and the mixture was heated under reflux condition for 3 h. Then the mixture was cooled down and the solvent was evaporated under vacuum. The obtained solid product was purified by recrystallization from alcohol to give 4-{[(6-chloro-1,3-benzothiazol-2-yl)-imino]-methyl}-benzoic acid (Intermediate).

STEP-2

To a solution of intermediate (0.02 mol) and 1-(4-hydroxyphenyl)-ethan-1-one (0.002 mol) in 40 ml of dichloromethane, dimethyl aminopyridine (0.002 mol) in 15 ml

DCM was added. Then the mixture was cooled down in an ice bath with constant stirring for 10 min. To this mixture, a solution of N,N'-dicyclohexylcarbodiimide (0.02) mmol was added dropwise. The mixture was stirred for 4 h at room temperature under continuous stirring. The solvent was removed under vacuum and the solid obtained was purified by column chromatography using a mixture of n-hexane/ethyl acetate (8:2) as eluent. The solid obtained was recrystallized from ethanol.

Preparation of IC (H-CD: L) in an aqueous medium

The Various concentrations of H-CD (0- 12×10^{-3} M) were prepared using double distilled water. The solution of compound (L) (1×10^{-3} M) was also prepared using double distilled water/DMSO in the ratio 8:2. Addition of the stock solution of compound (L) to different volumetric flasks followed by the addition of different concentrations of H-CD solutions ($0–12 \times 10^{-3}$ M) which were made up to the mark and then shaken thoroughly. These obtained solutions were used for absorbance and PL emission quantities. All the measurements were taken at room temperature.

Preparation of the solid IC (H-CD: L)

The **s**olid IC of compound L with H-CD was synthesized using reflux condition method. Firstly, 0.077 g of H-CD (1 mmol) in 50 mL of deionized water was continuously agitated using a magnetic stirrer at normal room temperature. Next, 0.022 g of compound (L) (1 mmol) was dissolved in 10 mL of deionized water/DMSO in the ratio 8:2 and added to the above mentioned aqueous H-CD solution. The mixture was poured into a round bottom flask and kept for reflux condition and continuously stirred for 24 h at 40 °C. The obtained complex was dried at 2 °C for 48 h. Subsequently, the obtained compound was filtered through a Whatman filter paper. Then the obtained IC was washed many times with double distilled water to expel unreacted compounds. Then the obtained IC was dried in the oven for 48 h at 50 °C and used for future studies.

Spectrofluorometric Determination of Hg²⁺ Ion in the IC

The stock solution of the IC (1×10^{-3} M) and a suitable aliquot of mercury metal ion Hg^{2+} (1×10^{-8} M) were dissolved by using deionized water and it was transferred into 10 ml standard volumetric flask and diluted to the mark. The solutions were mixed thoroughly and the photoluminescence (PL) intensity was measured at 318 nm on exciting the sample at 291 nm (Scheme 1).

Cell Incubation

L929 cells is an established and well-characterized cancer cell line that has demonstrated high reproducible results. L929 were cultured in modified Eagle's medium (MEM) supplemented with fetal bovine serum at 37 °C consisting 5% CO_2 in an air incubator. L929 cell lines were cultured on a 96-well plated culture medium with a concentration of 1×10^5 cell per well. The cultured cells were further treated with H-CD: L complex (0, 25, 50, 75, 100 µg concentrations in PBS buffer) for 3–4 h with MTT(3-(4,5-dimethylthiazol-2-yl)-2,5-diphenyl tetrazolium bromide) assay. After the incubation, the cells were washed with PBS buffer 3–5 times, and DMSO was added to solvate the formazan crystals to confirm that the non-availability of the H-CD: L in the additional region. The H-CD: L treated cells were further treated with Hg^{2+} ions in various concentrations (control and 50 µM) for 10 min and the obtained cells were subjected to fluorescence imaging. The confocal microscope images were observed at an excitation wavelength of 570 nm and the images were captured using a fluorescence microscope.
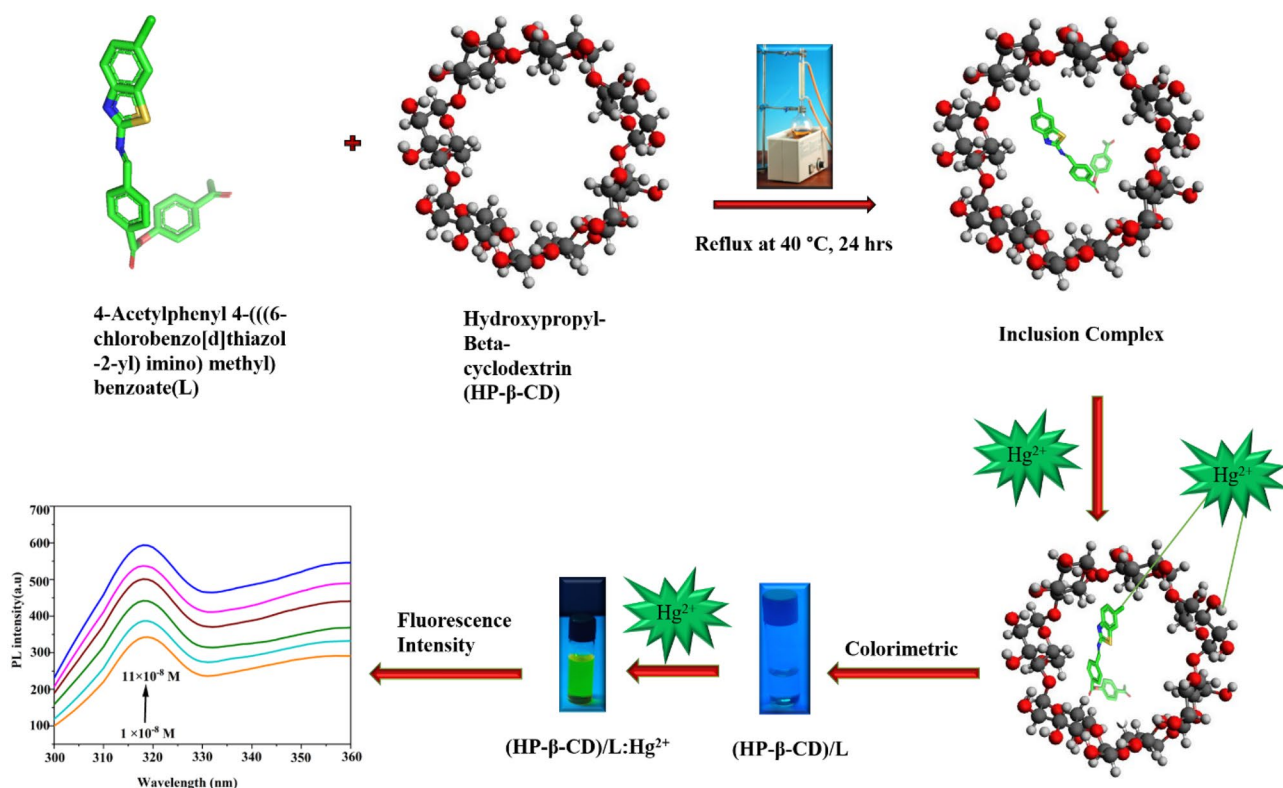
Results and Discussion

Solvatochromic Studies for the Compound L

Influence of Various Organic Solvents on PL Excitation and Emission Spectra

The absorbance and the PL spectra were obtained in different solvents of varying polarity (Fig. 1a, b). Table 1 gives the spectroscopic data of compound L in various solvents.

Maximum UV–visible absorption and PL wavelength of compound L were identified in the range 314–334 and 630–678 nm respectively in the selected solvents. On enhancing solvent polarity considerable redshifts was observed. A significant red shift ranging upto 48 nm was observed in the PL emission spectra of compound L. This is an indication to affirm the influence of solvent polarity on the energy of the singlet excited state. On increasing the solvent polarity Stoke's shift values enhanced from 15,974 cm⁻¹ to 16,298 cm⁻¹ for n-hexane to butanol respectively. This remarkable bathochromic redshift reveals that in polar solvents, the molecule acquires higher stabilty in a singlet excited state than in the ground state.

Solvent functions F_1, F_2, F_3 are employed in the Bakhshiev [25], Lippert-Mataga [26], and Kawski- Chamma- Viallet [27] equations respectively (Table 2).

Scheme 1 Schematic representation of the inclusion complex between Hydroxypropyl betacyclodextrin and Compound L

Determination of the Experimental and Theoretical Ground State and Excited State Dipole Moments

Linear correlations for solvent polarity methods proposed by Bilot-Kawski, Lippert-Mataga, Bakhshiev, Kawski-Chamma-Viallet, and Reichardt (Fig. 2) were used to obtain the experimental value of singlet excited state dipole moment. Stoke's shift (υ_A-υ_F) and its mean (υ_A + υ_F) / 2 were plotted against polarity functions $F_1(\varepsilon,n)$, $F_2(\varepsilon,n)$, $F_3(\varepsilon,n)$ (Table 3).
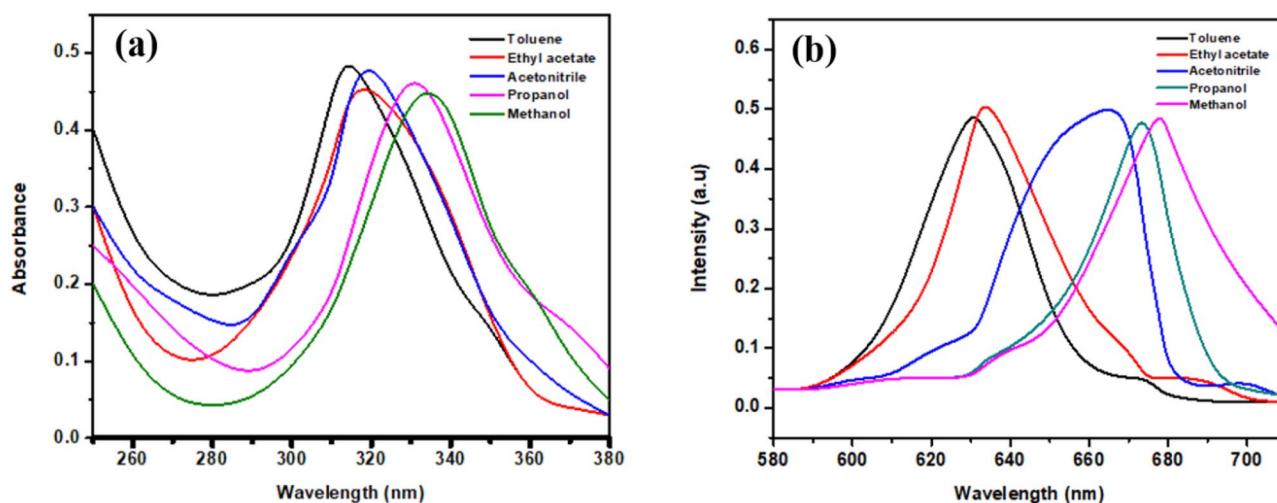

Fig. 1 (**a**) Absorbance spectra of compound L in different organic solvents (**b**) Emission spectra of compound L in various organic solvents

Table 1 Spectroscopic data of compound L in various solvents

Organic Solvents	l_a (nm)	l_f (nm)	$\bar{v}_a$ (cm^{-1})	$\bar{v}_f$ (cm^{-1})	$\Delta\bar{v}$(cm^{-1})	$(\bar{v}_a + \bar{v}_f)/2$
Toluene	314	<u>630</u>	31,847	15,873	15,974	23,860
1,4 Dioxane	315	633	31,746	15,797	15,998	23,771
Ethyl acetate	316	644	31,645	15,527	16,117	23,586
DCM	319	654	31,446	15,290	16,156	23,368
DMSO	320	660	31,350	15,151	16,198	23,250
Acetonitrile	321	668	31,152	14,970	16,182	23,061
Butanol	326	673	31,055	14,858	16,298	22,957
Propanol	328	674	30,487	14,836	15,651	22,662
Ethanol	330	676	30,303	14,792	15,510	22,547
Methanol	334	678	29,940	14,749	15,190	2234

Interaction of H-CD with L in the Aqueous State

UV–Visible Absorption Spectral Analysis of Compound L in H-CD

Development of a supramolecular IC with compound L and hydroxypropyl beta-cyclodextrin has been identified and analysed by using a UV–Visible absorption spectrum. The inclusion of guest molecule (compound L) into host molecule (H-CD), which reduce the number of water molecules. The complex behaviour depends on the particular structural (shape fit, charge fit, size fit) features of guest (compound L) and host molecules. The absorbance of compound L increases while adding different concentrations of H-CD (0–0.012 M) (Fig. 3a). In general, for different concentrations of H-CD, the absorbance range increases in the UV spectrum due to improved dissolution and encapsulation of compound L into H-CD non-polar cavity via hydrophobic interaction. Then the

equilibrium equation for solid IC formed between guest and host molecule (H-CD: L) can be written as,

$$H - CD + L \rightleftharpoons H - CD \dots\dots L \tag{1}$$

$$\frac{1}{A - A_0} = \frac{1}{\Delta\varepsilon} + \frac{1}{K[L] + \Delta\varepsilon[H - CD]^2} \tag{2}$$

By employing the Benesi–Hildebrand [25] equation for the inclusion host–guest complex (H- CD: L) determines the binding constant 'K' and stoichiometric ratios, where, A is the absorbance of compound L in the presence of H-CD and A_0 is the absorbance of compound L in the absence of H-CD, molar absorption coefficient (Δ_ε), [L] and [H-CD] are the initial concentration of compound L and H-CD respectively. Figure 3 (b, c) shows the plot of $1/A-A_0$ vs $1/$ [H-CD]^2 for compound L, a better linear range observed confirms the successful formation of the solid IC (H-CD). The binding constant 'K' was found to be 0.03 M^{-1}.

Table 2 Values obtained for solvent polarity functions through diverse correlation methods

Solvents	$F_1 (\varepsilon,n)^a$	$F_2 (\varepsilon,n)^b$	$F_3 (\varepsilon,n)^c$	ε^d	n^e
Toluene	0.01531	<u>0.03339</u>	0.34568	2.37	1.487
1,4 Dioxane	0.02150	0.04361	0.30848	2.22	1.422
Ethyl acetate	0.20072	0.49254	0.54878	6.08	1.372
DCM	0.21835	0.59496	0.49958	9.08	1.424
DMSO	0.26398	0.84210	0.74329	47.24	1.477
Acetonitrile	0.31538	0.8600	0.666	38.50	1.354
Butanol	0.26856	0.745	0.6573	19.84	1.426
Propanol	0.27249	0.7712	0.67212	21.80	1.424
Ethanol	0.29976	0.8170	0.6545	27.33	1.37
Methanol	0.30870	0.856	0.65200	35.10	1.33

ε = dielectric; ^{e}n = refractive index

^{a}Lippert-Mataga solvent function

^{b}Bakhshiev solvent function

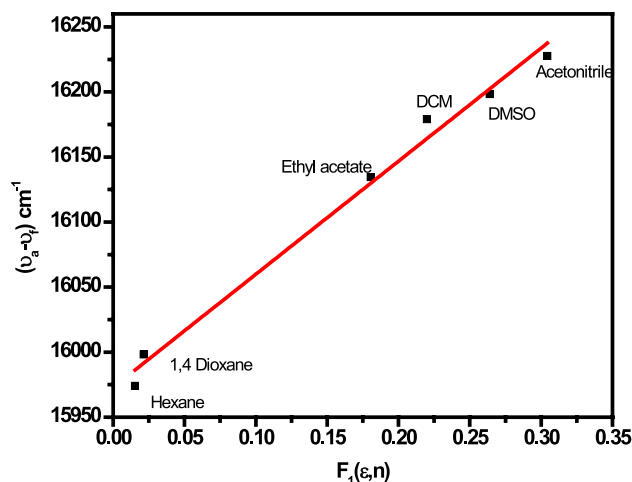^{c}Kawski-Chamma-Viallet solvent function

Fig. 2 The variation of Stoke's shift with $F_1(\varepsilon, n)$ using Lippert-Mataga equation for compound L

Table 3 Statistical analysis of the correlations of various solvent spectral shifts of Compound L

Correlations	Compound	Slope	Correlation factor 'r'	Number of data
Lippert-Mataga	L	869.11	0.9721	6
Bakhshiev	L	317.96	0.9636	7
Kawski-Chamma	L	-1965.23	0.9099	8

Ground-State dipole moment $\mu_g = 3.53D$

Excited-State dipole moment $\mu_e = 4.71D$

The ratio between the excited state and the ground state dipole moment is $(\mu_e/\mu_g) = 1.33D$

Calculated excited-state dipole moment (μ_e) from Lippert-Mataga equation = 5.06D

Calculated excited-state dipole moment (μ_e) from Bakhshiev's equation = 4.45D

Calculated excited-state dipole moment (μ_e) from Kawski-Chamma-Viallet's equation = 4.67D

PL Spectral Properties of Compound L in H-CD Medium

The interaction of H-CD and compound L was analysed using PL spectroscopy. In the emission spectra of compound L (Fig. 4a), the photoluminescence intensity increases gradually with the variation in H-CD concentration from 0 to 12×10^{-3} M. The obtained results show that compound L is encapsulated into the H-CD hydrophobic cavity to form H-CD: L solid IC. The fluorescence emission spectrum was found to be at 309 nm. The binding constant 'K' for the solid IC was calculated with the difference in maximum emission intensity by varying the H-CD concentration using the Benesi- Hildebrand equation [28] (Fig. 4b, c).

$$\frac{1}{I - I_0} = \frac{1}{I' - I_0} + \frac{1}{K[I' - I_0] + [HP - \beta - CD]^2} \quad (3)$$
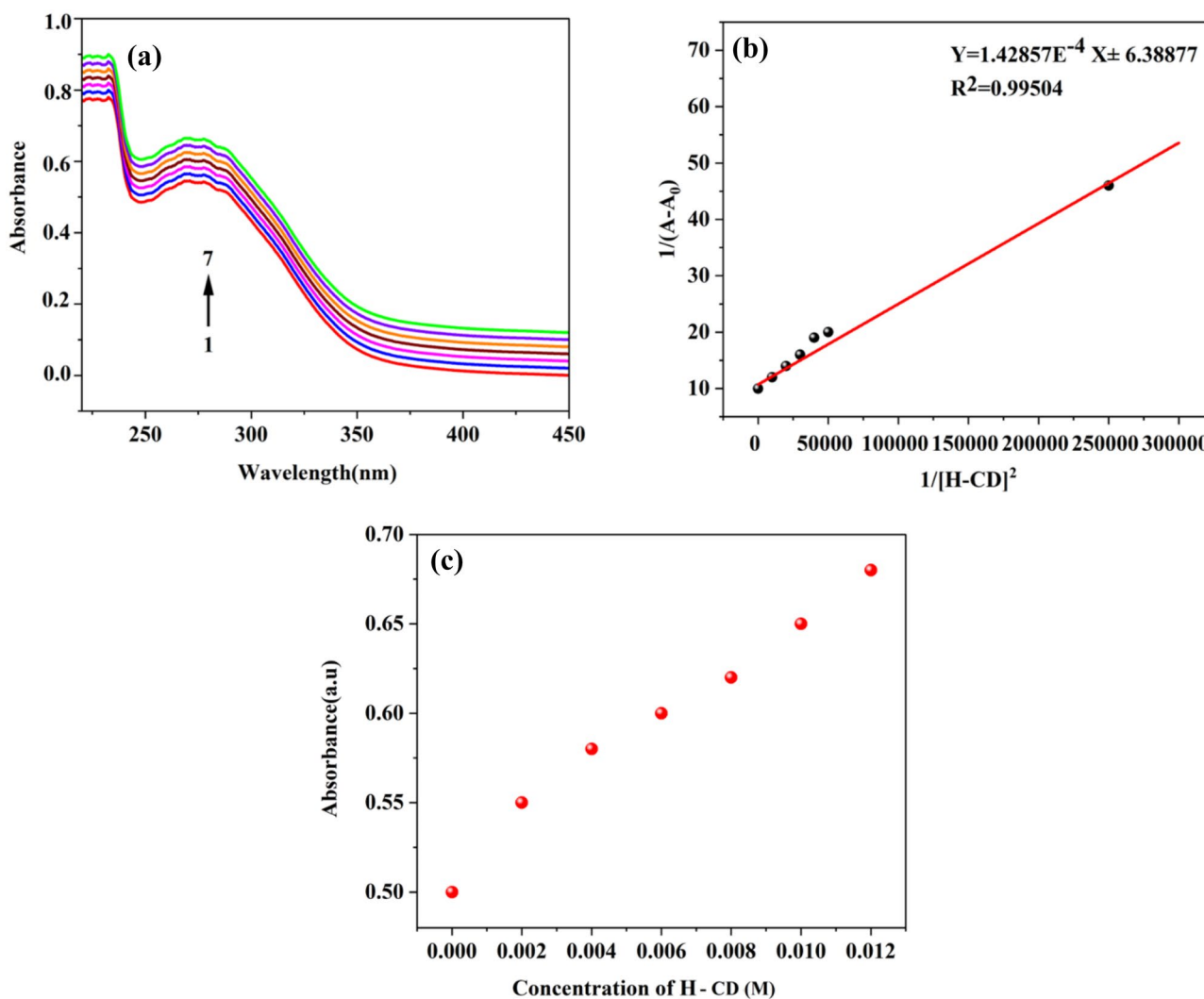

Fig. 3 (**a**) Absorption spectra of compound L (1×10^{-3} M) in various H-CD concentrations: (1) 0 M (2) 2×10^{-3} M (3) 4×10^{-3} M (4) 6×10^{-3} M (5) 8×10^{-3} M (6)10×10^{-3} M and (7) 12×10^{-3} M; (**b**) Graph of Benesi–Hildebrand plot $1/(A-A_0)$ vs. and (**c**) Absorption range of compound changes at 290 nm
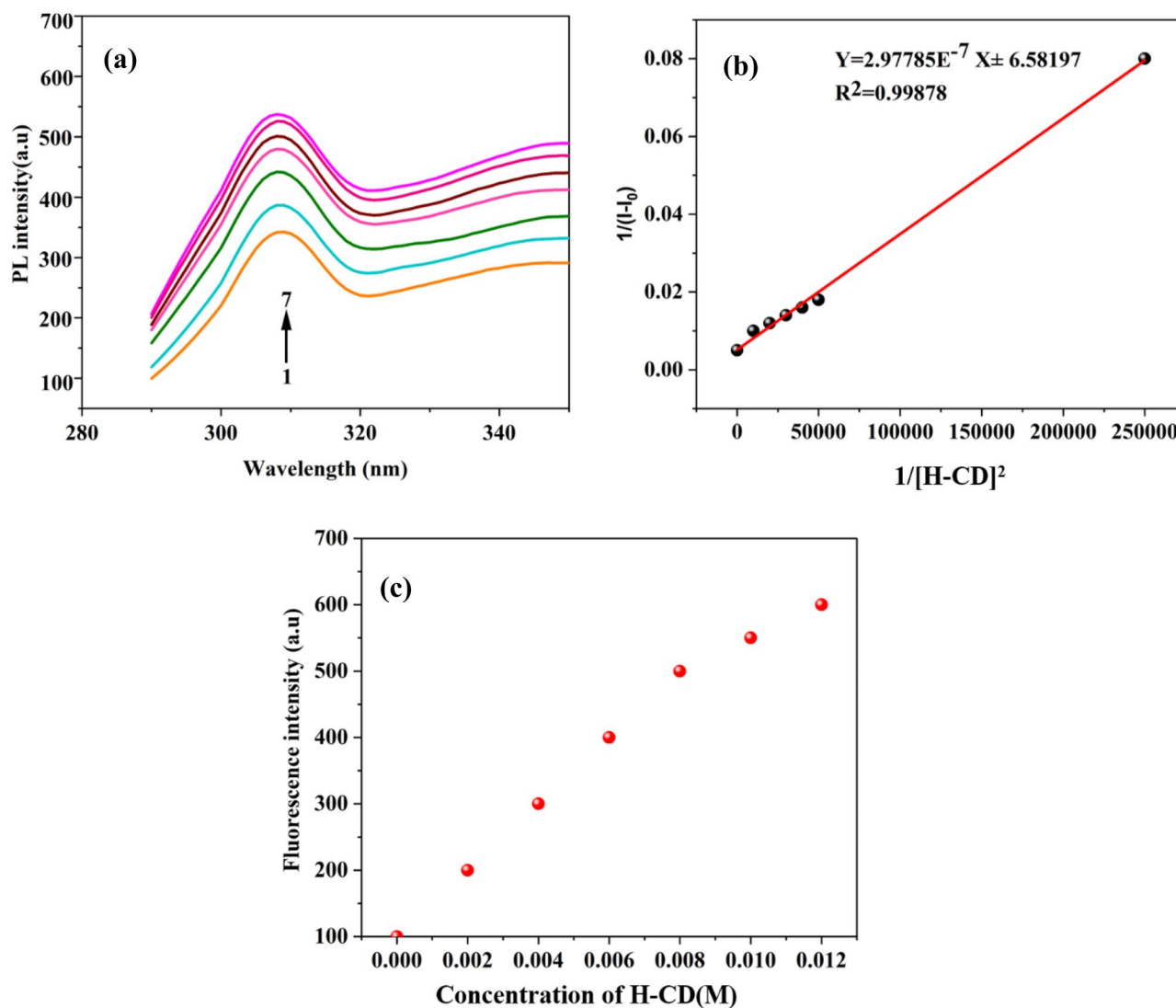
Fig. 4 (**a**) PL spectra of compound L (1×10^{-3} M) in various H-CD concentrations: (1) 0 M (2) 2×10^{-3} M (3) 4×10^{-3} M (4) 6×10^{-3} M (5) 8×10^{-3} M (6) 10×10^{-3} M and (7) 12×10^{-3} M; (**b**) Graph of Benesi–Hildebrand plot $1/(I - I_0)$ vs. $1/$ [H-CD] and (**c**) PL intensity range of compound L changes at 309 nm

where $[\text{H-CD}]^2$ represents the H-CD concentration, I and I_0 were the PL intensities of compound L in the absence and presence of H-CD respectively, I ′ is the limiting intensity. The binding constant 'K' found to be 0.0335 M^{-1}.

Characterisation of Compound (L) with H-CD in Solid-State

FT-IR Spectral Analysis

FT-IR spectral analysis was employed to study the hydrophobic host–guest complex interactions between H-CD and compound L. The spectrum of hydroxy-propyl-beta cyclodextrin, compound L, and IC (H-CD: L) is depicted in Fig. 5. The characteristic absorption frequency range for H-CD was observed at 3345 cm^{-1} (O–H stretching band), 2897 cm^{-1} (C-H stretching band), 1640 cm^{-1} (bending O-H band), 1418 cm^{-1} (deformation O–H), 1151 cm^{-1} (C-O-C stretching band), 1014 cm^{-1} (C-C-O stretching band), 947 cm^{-1} (α-1,4 linkage skeletal band), 854 cm^{-1} (C-O, C-C, C-C-H from anomeric band) [29].

4-Acetylphenyl4-(((6-chlorobenzo[d]thiazol-2-yl)-imino)-methyl)-benzoate IR frequency range was observed at 3405 cm^{-1} (stretching N–H band), 3090 cm^{-1}
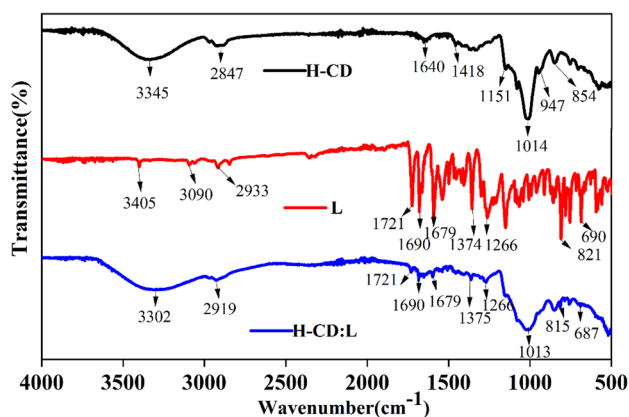
Fig. 5 FT-IR spectrum of H-CD, L and H-CD: L

Fig. 6 Raman spectra of H-CD, compound L, and H-CD: L complex

(aromatic C-H stretching band), 2933 cm^{-1}(asymmetric C-H stretching band), 1721 cm^{-1}(stretching O-C=O vibration),1690 cm^{-1}(C=N stretching band),1679 cm^{-1}(stretching C=O band), 1266 cm^{-1} (stretching C-N band), 690 cm^{-1} (stretching C-S band) and bending band of ν(C-H) at 1374 cm^{-1}, and halo compound ν(C-Cl) observed at 821 cm^{-1} respectively. The range of ν(OH), ν(CH$_2$) in H-CD 3345 cm^{-1}, 2897.23 cm^{-1} was shifted to 3302 cm^{-1}, 2919 cm^{-1} in the solid IC. Bands at 1721 cm^{-1}, 1690 cm^{-1},1679 cm^{-1}, 1266 cm^{-1}, 821 cm^{-1}, 690 cm^{-1} which corresponds to stretching vibration of ν(O-C=O), ν(C=N), ν(C=O), ν(C-N), ν(C-Cl), ν(C-S), and bending vibration of ν(C-H) at 1374 cm^{-1} of 4-acetylphenyl benzoate
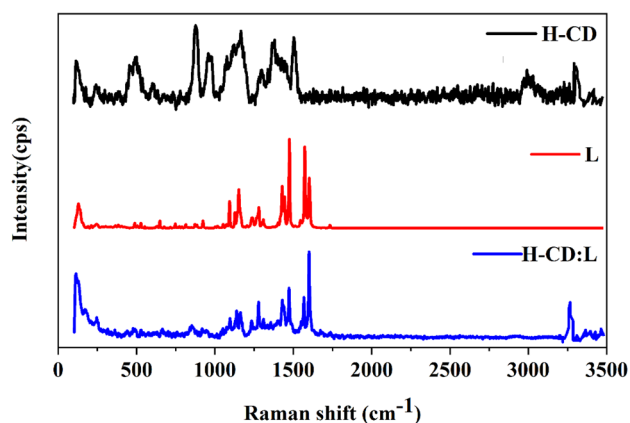
appeared in the IC. This result proves that the developed solid IC was confirmed.

Raman Spectral Analysis

Raman spectroscopy is employed to describe the width and intensity of the molecular structures [30]. The Raman spectrum of compound L, H-CD, and H-CD: L complex were characterized in Fig. 6 and the assignments of peaks are tabulated in Table 4.

The vibrations of ν (C=C), δ (C-C), δ (C-H), and ν(C-N) appeared at 1614 cm^{-1}, 1582.66 cm^{-1}, 1470 cm^{-1}, and 1285 cm^{-1} respectively. The ring deformation of ν (C-C)

Table 4 FT Raman band assignments of compound L, H-CD, and the solid IC (H-CD: L)

Compound L (cm^{-1})	Complex (cm^{-1})	Assigned peak	H-CD (cm^{-1})	Complex (cm^{-1})	Assigned peak
1614	1605	ν (C=C)	3323	3266	ν (O-H)
1582	1582	ν (C=C)	2935	2934	ν (C-H)
1472	1472	ν (C-C); δ (C-C)	1468	1418	δ (C-H)
1334	1333	ν (C-C); Ring deformation	1393	1363	δ (O-H)
1285	1285	ν (C-H)	1340	1301	δ (C-H)
1246	1246	ν (C-C); δ (C-H)	1263	1238	δ (C-H)
1144	1144	δ (C-H); ν (C-C)	1134	1125	ν (C-C)
1020	1020	ν (C-C)	1051	1046	ν (C-O)
236	195	C-NH out of plane bending	942	941	ν (C-O)
			855	855	Breath of glucose ring
			761	762	In-plane deformation
			580	580	ν (O-H)
			489	480	In plane deformation of glucose ring

and C-NH out of plane bending peaks appear at 1334 cm^{-1} and 236 cm^{-1} respectively Raman spectrum of hydroxypropyl beta-cyclodextrin, ν(O-H) vibration was observed at 3323 cm^{-1} because of the high number of intramolecular and intermolecular hydrogen bonds. The ν (C-H) vibration of CH$_2$ showed at 2935 cm^{-1} and the vibration of δ (O-H) appeared at 1393 cm^{-1}. The δ(C-H) vibrations appeared at 1468, 1340, 1263 cm^{-1}. The vibration of ν (C-O) were found to be 1051, 1042 cm^{-1}. The deformation in-plane glucose ring was identified at 761 and 489 cm^{-1} respectively.

The H-CD ν (O-H) vibration 3323 cm^{-1} was shifted to a lower wavenumber 3266 cm^{-1} in the solid IC. Similarly, the ν (C=C) vibration and the C-NH out of plane bending vibration in compound L shifts also shifts to a lower wavenumber. The obtained results clearly explained that the compound L is incorporated in the cavity of H-CD.

Nuclear Magnetic Resonance Spectral Analysis (^{1}H NMR)

^{1}H NMR is one of the significant methods used to decide the sub-atomic interaction among host and guest particles [31, 32]. Essentially, ^{1}H NMR results depends on the perception of specific line enlargement or chemical shift ($\Delta\delta$) relocation of guest (compound L) and host (H-CD) protons. Indeed, that critical compound shift happens just for hydrogens (H) present on the inward surface protons (H3 and H5) of the H-CD, and not exactly for the external environment protons (H1, H2, H4, and methylene H6), which allows one to build up clearly, that these progressions are the product of solid IC (H-CD: L) development and not the non-specific interaction among the two molecules [33, 34]. ^{1}H NMR spectroscopy has been utilized for quite a long time to acquire cyclodextrin IC binding mode data, and as of recently, it is one of the major strategies for solid IC study [35–37].

As for the compound L, it couldn't be disintegrated in deionized water by any means. Hence, a few scientists, Chirag et al. chose a solvent DMSO for ^{1}H NMR spectra when they met the comparative issue [38, 39]. The ^{1}H NMR spectra of guest molecule, host molecule and IC (H-CD: L) are shown in Fig. 7. The chemical shifts of H-CD free protons and H-CD: L complex are shown in Table 5, the chemical shifts were measured by using the following equations:

$$\Delta\delta = \Delta\delta(IC) - \Delta\delta(H - CD)$$
$$\Delta\delta = \Delta\delta(IC) - \Delta\delta(L) \tag{4}$$

In this arrangement, positive(+ve) and negative(-ve) chemical shifts show upfield and downfield shifts, respectively. Table 5 shows that the protons H3 and H5, placed inside the hydrophobic environment of H-CD, obviously move towards the upfield direction, related with the minor upfield shifts of protons H2 and H4, which are present in exterior of the cavity. This confirms that the encapsulation between the compound L and the interior environment of the H-CD cavity.

X-ray Diffraction (XRD)

X-ray diffractometry (XRD) is used to study the physical properties (i.e., crystalline or amorphous) of the host–guest solid IC molecules. H-CD, compound L, and H-CD: L (solid IC), XRD patterns were depicted in Fig. 8. The XRD patterns of H-CD, showed no obvious characteristic diffraction peaks. It exhibits one broad diffraction peak band around 20°, indicating that the H-CD is in an amorphous nature [40]. The compound L exhibits sharp peaks indicating the crystalline nature of the guest molecule. The sharp peaks in compound L and broad diffraction peaks in host molecule H-CD are shown in H-CD: L (IC). This confirms that the compound L is encapsulated in the H-CD cavity and as well as it suggests that the solid IC H-CD: L is amorphous.

Scanning Electron Microscope (SEM)

Scanning electron microscope (SEM) is one of the qualitative methods, used to analyse the morphological features of the host (H-CD), guest molecules (compound L) and their solid IC (H-CD: L). The morphological structure of H-CD, compound L and solid IC (H-CD: L) are shown in Fig. 9. Typical amorphous structures of H-CD and crystal structure of compound L are originated in various sizes. The solid IC (H-CD: L) is found to be an amorphous moiety and homogeneous in nature. Hence, the differences in shape and size of H-CD: L compared to the parent compound, confirms the development of the H-CD: L solid IC.

Characterisation of compound (L) with H-CD in the Theoretical State

Molecular Docking Technique

Binding cavity of the H-CD was docked into compound L. Then the obtained results were represented in Fig. 10.
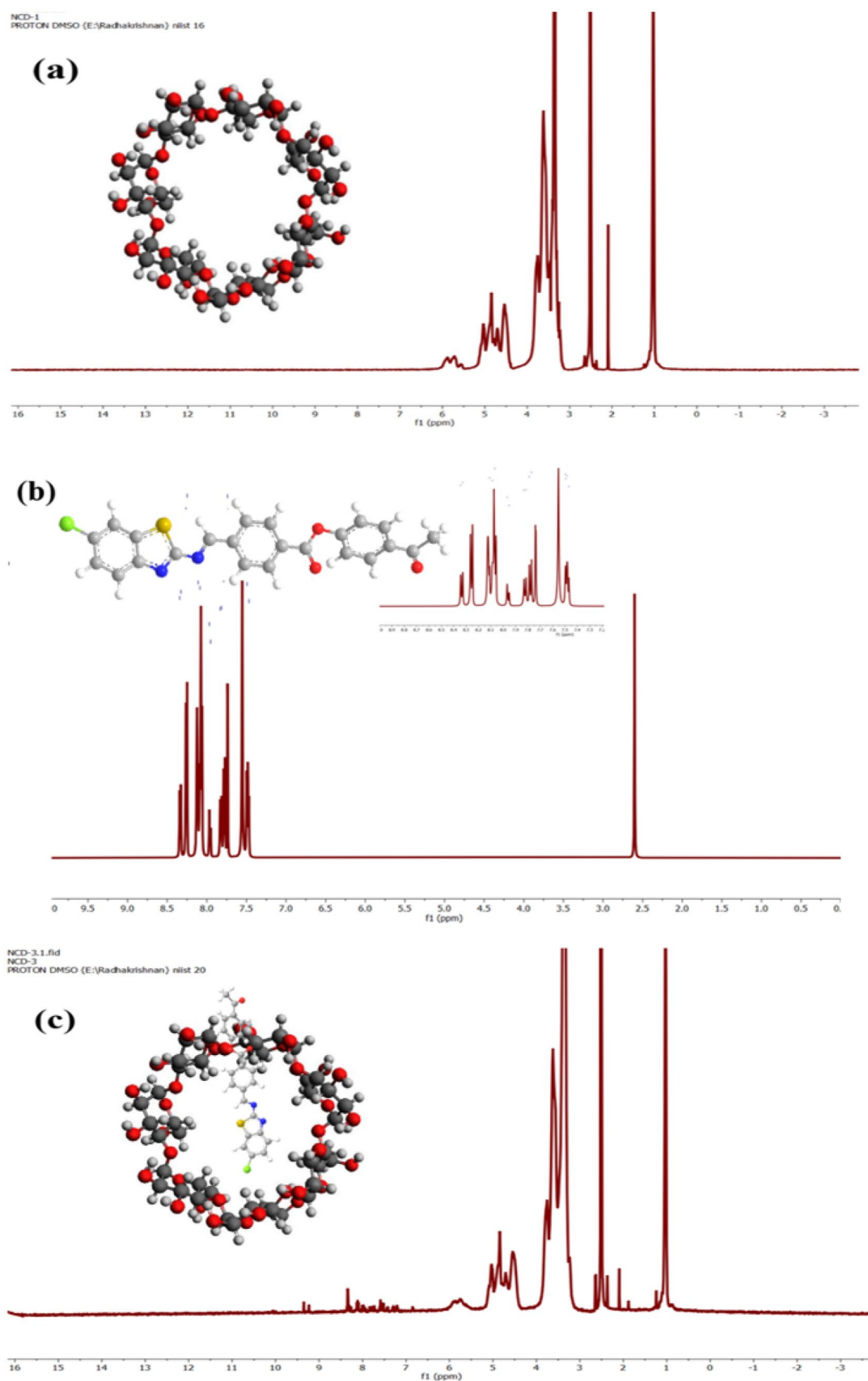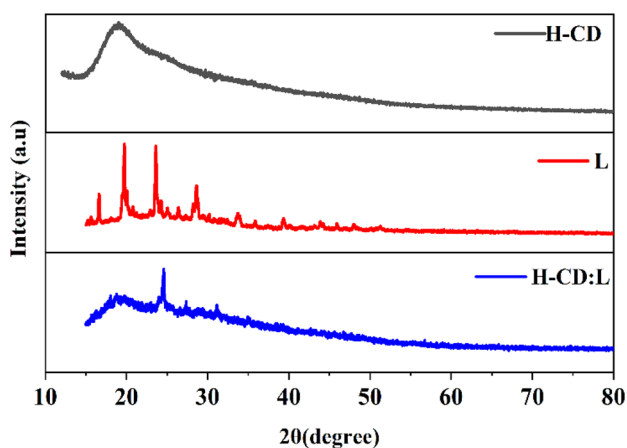
Fig. 7 ¹H NMR spectra of (**a**) H-CD (**b**) Compound L (**c**) the solid IC of H-CD: L

Table 5 Change in ^{1}H NMR chemical shift values of compound L and H-CD in free and IC states (H-CD: L) determined in DMSO-d6 at 298 K

Substance	H-Protons	Free (δ, ppm)	IC (δ, ppm)	$\Delta\delta$(ppm)
H-CD	1	5.16	5.09	–0.07
	2	3.767	3.736	–0.031
	3	3.925	3.856	–0.069
	4	3.400	3.35	–0.05
	5	3.626	3.520	–0.106
	6	3.50	3.47	–0.03
Compound L	a	7.55	7.45	–0.1
	b	7.74–7.73	7.65	–0.09
	c	8.12–8.06	8.04	–0.08
	d	8.35–8.32	8.24	–0.11
	e	7.83–7.75	7.65	–0.18
	f	8.27–8.24	8.20	–0.04
	g	7.50–7.49	7.47	–0.03
	h	7.97–7.95	7.93	–0.04
	i	2.46	2.40	–0.06

The 3D diagram of compound L and H-CD were individually exposed in Fig. 10a, b. The calculated binding energy between the compound L and H-CD was found to be -5.9 kcal mol^{-1}. The compound L accepted a solid conformation and it was wrapped by H-CD. This encapsulation helped compound L to anchor to the binding site of H-CD. Docking studies were performed using Auto dock Vina software and PyMol software was used for visualization. The above molecular simulations provided a rational explanation of the interactions between the compound L and H-CD. Further, provided that reasonable data about the mode of action of the H-CD: L solid IC.

Fig. 8 XRD diffraction of H-CD, compound L, and H-CD: L complex

Analytical Application of H-CD: L Probe as a Fluorescence Sensor for Hg^{2+} Detection

Ability of Metal Sensing Towards IC

During the formation of IC, the PL techniques showed a continual enhancement in the intensity of H-CD: L complex which acts as an important factor for chemosensory applications. Hence, to estimate the IC chemical sensing ability, the PL emission spectra of IC were recorded using different heavy metal ions to identify the metal sensing behaviour of the IC. Figure 11 (a, b) displays that the PL emission spectra of IC in the metal free (absence) and the presence of various metal ions such as Ag$^+$, Co^{2+}, Cr^{3+}, Cs$^+$, Hg^{2+}, Ba^{2+}, Mg^{2+}, Fe^{2+}, Fe^{3+}, K$^+$, Na$^+$. It was observed that on addition of heavy metal cations to IC (H-CD: L) produced no noteworthy change, whereas on addition of Hg^{2+} showed an enhanced PL intensity.

Selectivity Study for the IC Towards Hg^{2+}

PL spectra of H-CD: L IC+heavy metal ions (as Ag$^+$, Co^{2+}, Cr^{3+}, Cs$^+$, Hg^{2+}, Ba^{2+}, Mg^{2+}, Fe^{2+}, Fe^{3+}, K$^+$, Na$^+$) were analysed. Figure 11 c shows that the PL intensity increased on the addition of Hg^{2+} on the fluorescent probe (H-CD: L complex) and not influenced by the presence of other heavy metal ions. This result shows that the IC probe has a very high selective on Hg^{2+}. Later, the H-CD: L IC used as a chemosensor for Hg^{2+} sensing in the aqueous medium. PL emission spectra of IC with various concentrations of Hg^{2+} were analysed to obtain the sensitivity of fluorescent probe. Figure 11 d displays the PL spectrum of various concentrations of an analyte. The emission intensity was found to be 317 nm on the addition of the analyte. The limit of quantitation was calculated using (10 σ)/s and was found to be 8.13×10^{-10} M (Table 6). The linear dynamic range of H-CD: L complex + analyte is 1×10^{-8} M – 11×10^{-8} M and the detection of limit was found to be 2.71×10^{-10} M (Fig. 11 e). The plausible mechanism for the PL enhancement of IC fluorescent probe with Hg^{2+} ions is shown in Scheme 2.

Detection of Hg^{2+} in Live Cells

Biosensing of target molecules to selectively observe guest species in living cells are of excessive significance for biological applications [44]. The cell viability and cytotoxicity assay were investigated in L929 cells by using MTT assay as shown in Fig. 12 a. The cell viability of H-CD: L showed greater than 90% upon addition of H-CD: L with different concentrations ranging from
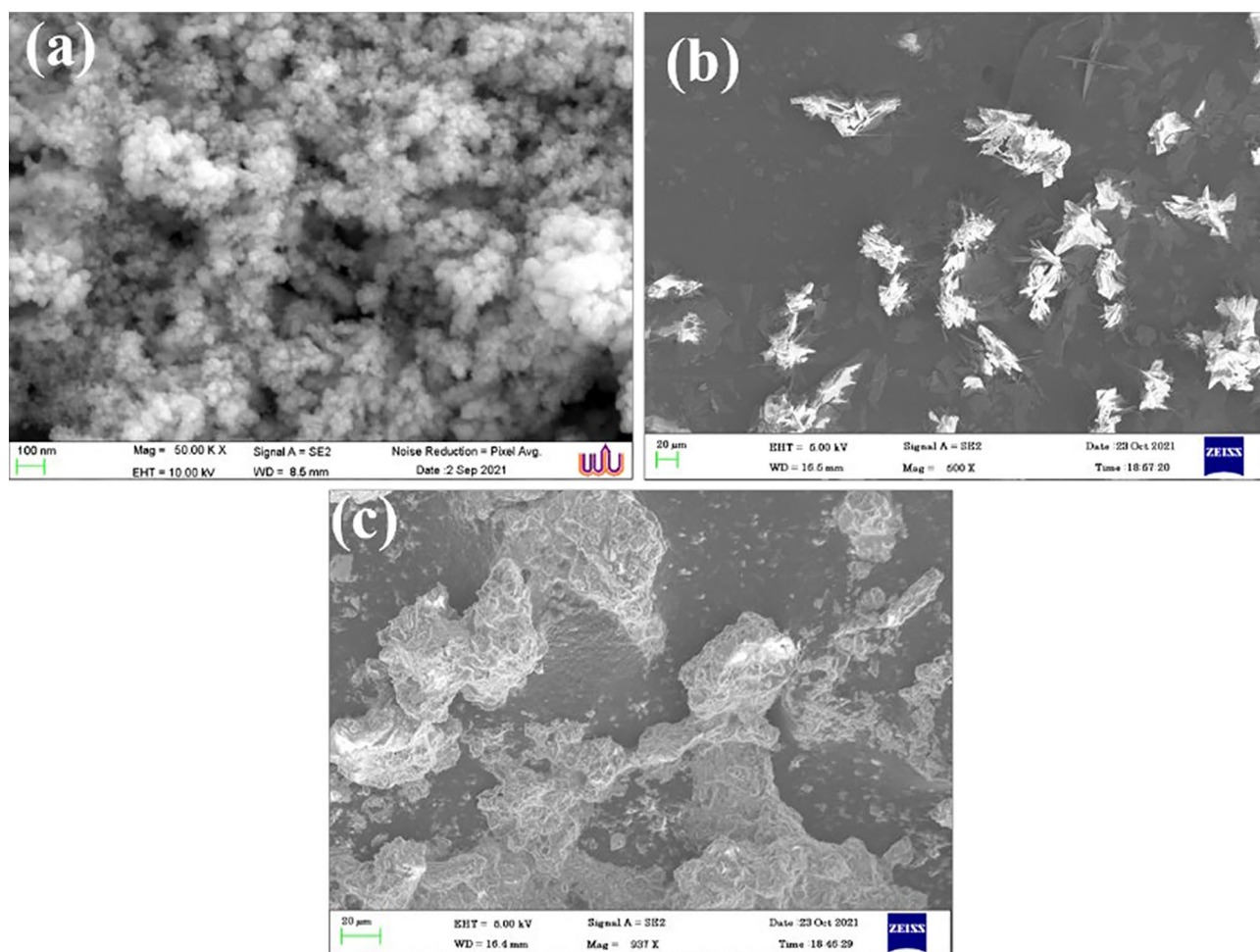
Fig. 9 SEM pictures of H-CD, compound L, and H-CD: L complex

0–100 µg/ml (24 h). The results confirmed that H-CD: L is non-toxic and bio-compatible. The synthesized H-CD: L and H-CD: L + analyte act as an excellent biological

Fig. 10 Structure of (**a**) H-CD, (**b**) compound L, and (**c**) H-CD: L complex

probe which was confirmed by fluorescence stability and cytotoxicity. Figure 12 b explains the fluorescence image of H-CD: L using L929 cells is considered as a further application. The fluorescence images of L929 cells were incubated with H-CD: L and H-CD: L + analyte. The fluorescence images were obtained by using the confocal microscope.
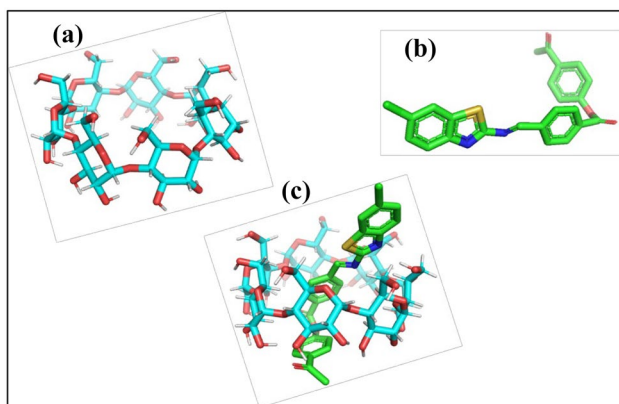
Real Water Sample Analysis

The proposed chemosensor H-CD: L was used for the detection of Hg^{2+} in drinking water, tap water and lake water samples. Different waters were investigated without any pre-treatment. All the water samples tests were spiked with H-CD: L IC at fixation level and investigated. The outcomes are displayed in Table 7. The recovery range of Hg^{2+} was found to be 97–101%. The developed fluorescent probe has been successfully applied for the detection of Hg^{2+} in real examples.
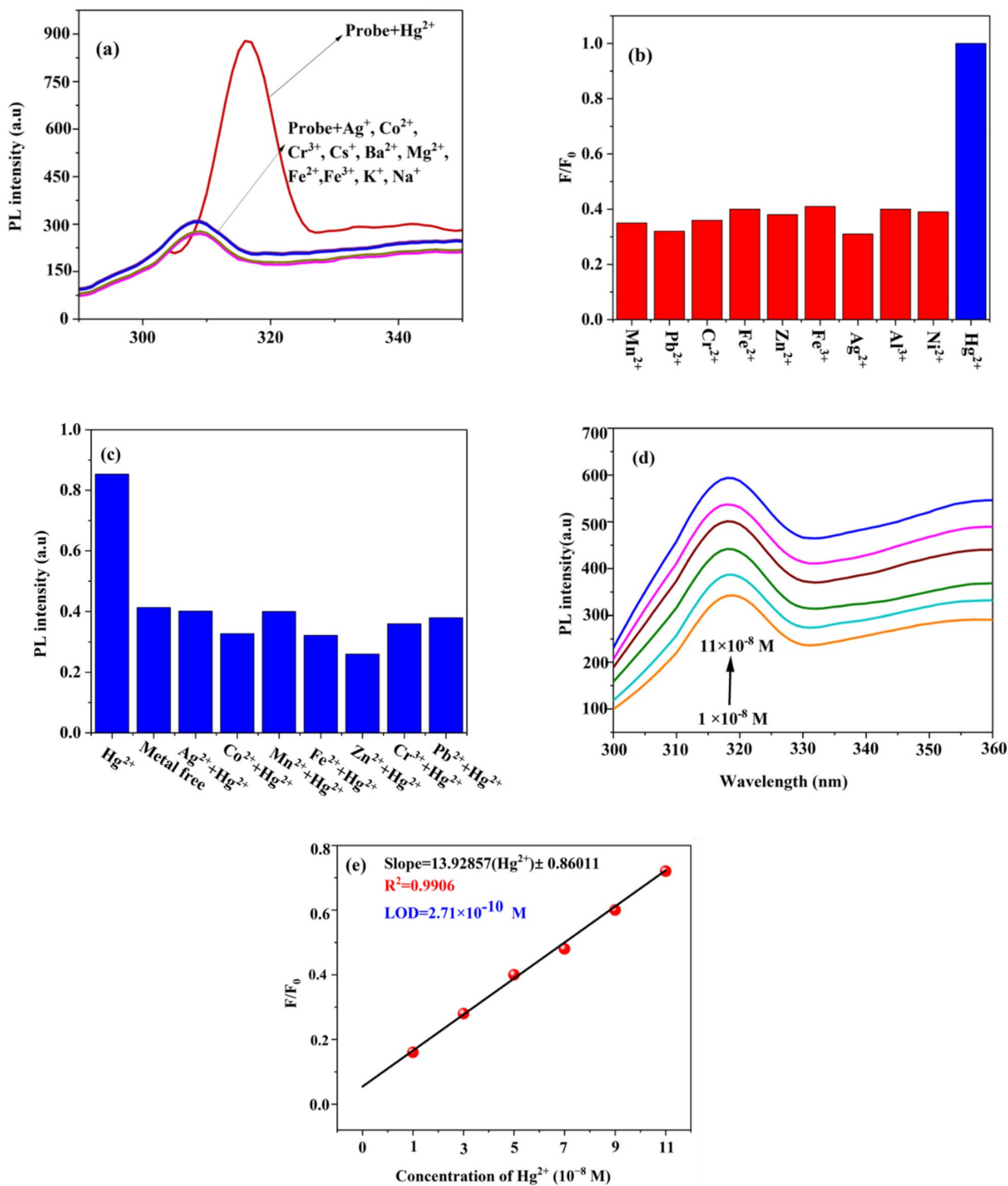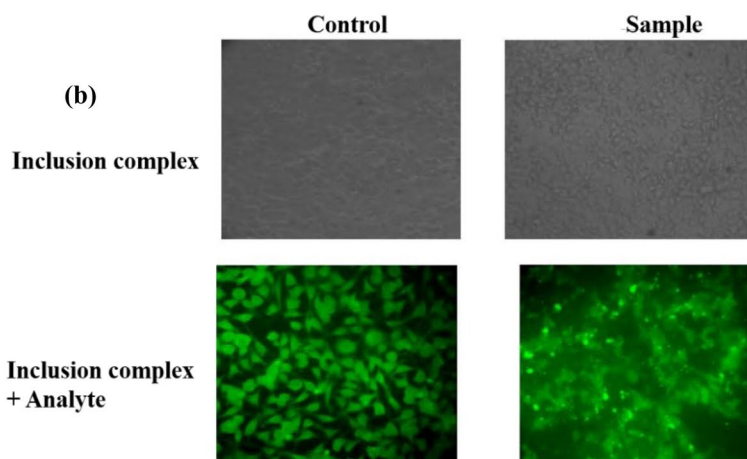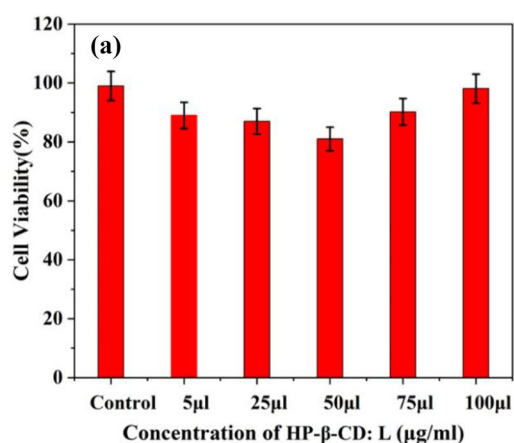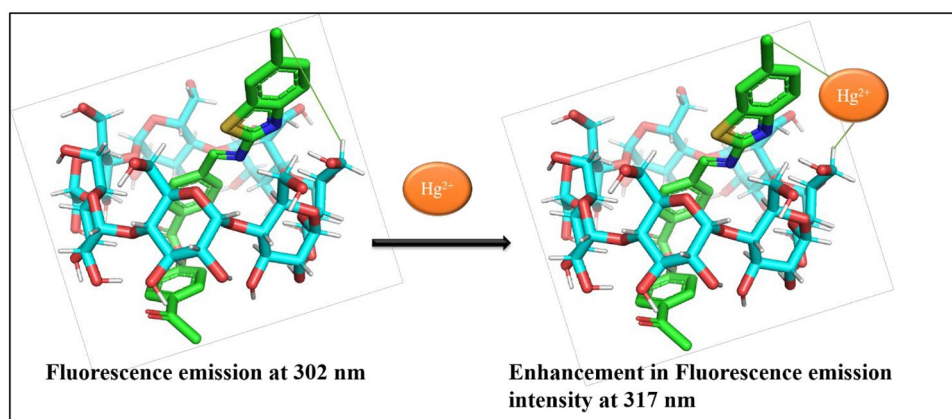
Fig. 11 (**a**) PL spectra of H-CD: L in the presence of the various metal cations (1×10^{-4} M) (**b**) PL intensity of H-CD: L IC in water in the presence of different metal heavy ions (1×10^{-4} M) (**c**) PL emission spectra of H-CD: L chemosensor [concentration of compound L 1×10^{-3} M, H-CD: 12×10^{-3} M] to 1×10^{-8} M Hg^{2+} in presence of other metal cations (10^{-8} M); (**d**) PL titration spectra of H-CD: L chemosensor in the presence of a different concentration of Hg^{2+} (**e**) Linear plot between PL intensity and concentrations of Hg^{2+} (1×10^{-8} -11×10^{-8} M)

Table 6 Proposed IC method compared with reported methods

Reported Methods	Reagents	Linear range	LOD	Ref
Voltammetric	2-Mercapto benzothiazole (2-MBT)	$5\times10^{-8} - 8\times10^{-7}$ M	1×10^{-8} M	[41]
Spectrophotometry	Meloxicam	1.0–15.0 mM	0.296 mM	[42]
Spectrophotometry	Azocarmine G	0.3–50.0 nM	0.125 nM	[43]
Spectro fluorimetry	β-CD: 2H1NA complex	$1\times10^{-4}- 2\times10^{-4}$ M	2.4×10^{-5} M	[30]
Spectro fluorimetry	H-CD: L	$1\times10^{-8}-11\times10^{-8}$ M	2.71×10^{-10} M	**This work**

Scheme 2 The plausible mechanism for the PL enhancement of probe H-CD: L with Hg^{2+}

Fluorescence emission at 302 nm

Enhancement in Fluorescence emission intensity at 317 nm

Fig. 12 (**a**) Cell viability assay of L929 cells incubated with different concentrations of H-CD: L. after 24 h (**b**) Confocal images of L929 cells incubated with different concentrations of H-CD: L and H-CD: L+analyte

Table 7 Real water sample analysis

Sample	Spiked concentration (nM)	Proposed method (nM)	RSD (%)	AAS method (nM)	RSD (%)
Tap water	0.0	30.10	1.00	30.26	0.80
	2.5	32.6	1.71	32.76	1.78
	5.0	35.1	0.87	35.26	0.95
Wastewater	0.0	18.18	0.66	18.15	0.76
	2.5	20.68	1.50	20.65	1.38
	5.0	23.18	0.78	23.15	0.85
River water	0.0	22.12	1.20	21.18	1.21
	2.5	24.62	0.72	23.68	0.88
	5.0	27.12	1.01	26.18	1.05

Conclusion

The formation of solid IC between 2-hydroxypropyl beta-cyclodextrin and compound L was identified through different states (i.e., solid, liquid and virtual state). The binding constants 'K' of the synthesized H-CD: L IC was investigated through UV–visible and PL spectral analysis. The solid IC was identified and confirmed by using XRD, Raman, SEM, NMR techniques. Molecular docking studies were performed to prove the successful formation of the IC theoretically. The sensing behaviour of the H-CD: L IC towards Hg^{2+} was identified using PL spectroscopy. The estimated LOD was found to be 2.71×10^{-10} M. The intracellular uptake of Hg^{2+} by H-CD: L IC was tested in the L929 cancer cell line which proved the complex to be non-toxic and biocompatible.

Author Contribution Keerthana P: Conceptualization, Methodology, Hanna Abbo: Methodology, Anila Rose Cherian: Conceptualization, Methodology, Salam Titinchi: Writing- Reviewing and Editing, Anitha Varghese: Writing- Reviewing and Editing.

Declarations

Ethics Approval Not applicable.

Consent to Participate Not applicable.

Consent for Publication Not applicable.

Competing Interests The authors have no competing interests with the work presented in this manuscript.

References

1. Moragues ME, Manez RM, Sancenon F (2011) Chromogenic and fluorogenic chemosensors and reagents for anions. A comprehensive review of the year 2009.Chem Soc Rev 40:2593–2643.https://doi.org/10.1134/S0020441220050139

2. Kim HN, Ren WX, Kim JS, Yoon J (2012) Fluorescent and colorimetric sensors for detection of lead, cadmium, and mercury ions. Chem Soc Rev 41:3210–3244. https://doi.org/10.1039/C1CS15245A

3. Cheng H, Hu Y (2012) Mercury in municipal solid waste in China and its control: a review. Environ Sci Technol 46:593–605. https://doi.org/10.1021/es2026517

4. Mahato P, Saha S, Das P, Agarwalla H, Das A (2014) An overview of the recent developments on Hg2+ recognition. RSC Adv 4:36140–36174. https://doi.org/10.1039/C4RA03594A

5. Akshaya KB, Reenamole G, Sasitharan K, Vinod TP, Varghese A, George L (2019) Trace level determination of Hg 2+ ions in environmental samples with a mercaptotriazole-functionalized TiO 2 nanostructure-based fluorescent probe. Anal Methods 11(4):537–547. https://doi.org/10.1039/C8AY02109K

6. Harris HH, Pickering IJ, George GN (2003) The chemical form of mercury in fish. Science, 301: 1203–1203. www.sciencemag.org/cgi/content/full/301/5637/1203/ DC1

7. Steere NV (1965) Mercury vapor hazards and control measures. J Chem Educ 42:529. https://doi.org/10.1021/ed042pA529

8. Foucher D, Hintelmann H, Al TA, MacQuarrie KT (2013) Mercury isotope fractionation in waters and sediments of the Murray Brook mine watershed (New Brunswick, Canada): Tracing mercury contamination and transformation. Chem Geol 33:87–95. https://doi.org/10.1016/j.chemgeo.2012.04.014

9. Gomathi A, Viswanathamurthy P (2019) Near-infrared fluorogenic switches for the detection of Hg (II) ions: applications in real samples and living cells. Anal Methods 11:2769–2777. https://doi.org/10.1039/C9AY00241C

10. Sam B, George L, Varghese A (2021) Fluorescein based fluorescence sensors for the selective sensing of various analytes. J Fluorescence 31(5):1251–1276. https://doi.org/10.1007/s10895-021-02770-9

11. Lee R, Middleton D, Caldwell K, Dearwent S, Jones S, Lewis B et al (2009) A review of events that expose children to elemental mercury in the United States. Environ Health Perspect 117:871–878. https://doi.org/10.1289/ehp.0800337

12. Mishra J, Kaur H, Ganguli AK, Kaur N (2018) Fluorescent chemosensor based on urea/thiourea moiety for sensing of Hg (II) ions in an aqueous medium with high sensitivity and selectivity: a comparative account on effect of molecular architecture on chemosensing. J Mol Struct 1161:34–43. https://doi.org/10.1016/j.molstruc.2018.01.004

13. Culzoni MJ, De La Peña M, Machuca A, Goicoechea H, Babiano R (2013) Rhodamine and BODIPY chemodosimeters and chemosensors for the detection of Hg 2+, based on fluorescence enhancement effects. Anal Methods 5:30–49. https://doi.org/10.1039/C2AY25769F

14. Khun NW, Liu E (2009) Linear sweep anodic stripping voltammetry of heavy metals from nitrogen doped tetrahedral amorphous carbon thin films. Electrochim Acta 54:2890–2898. https://doi.org/10.1016/j.electacta.2008.11.014

15. Pohl P (2009) Determination of metal content in honey by atomic absorption and emission spectrometries. TRAC-Trend Anal Chem 28:117–128. https://doi.org/10.1016/j.trac.2008.09.015

16. Zhou J, Tian Y, Wu X, Hou X (2017) Visible light photochemical vapor generation using metal-free g-C3N4/CQDs composites as catalyst: Selective and ultrasensitive detection of mercury by ICP-MS. Microchem J 132:319–326. https://doi.org/10.1016/j.microc.2017.02.016

17. Dhivya R, Kavitha V, Gomathi A, Keerthana P, Santhalakshmi N, Viswanathamurthi P, Haribabu J (2022) Dinitrobenzene ether reactive turn-on fluorescence probes for the selective detection of H 2 S. Anal Methods 14(1):58–66. https://doi.org/10.1039/D1AY01700D

18. Keerthana P, Cherian AR, Sirimahachai U, Thadathil DA, Varghese A, Hegde G (2022) Detection of picric acid in industrial effluents using multifunctional green fluorescent B/N-carbon quantum dots. J Environ Chem Eng. 14:107209. https://doi.org/10.1016/j.jece.2022.107209

19. Szejtli J (1998) Introduction and general overview of cyclodextrin chemistry. Chem Rev 98:1743–1754. https://doi.org/10.1021/cr970022c

20. Loethen S, Kim JM, Thompson DH (2007) Biomedical applications of cyclodextrin based polyrotaxanes. J Macromol Sci Polymer Rev 47:383–418. https://doi.org/10.1080/15583720701455145

21. Hedges AR (1998) Industrial applications of cyclodextrins. Chem Rev 98:2035–2044. https://doi.org/10.1021/cr970014w

22. Ogoshi T, Harada A (2008) Chemical sensors based on cyclo-dextrin derivatives. Sensors 8:4961–4982. https://doi.org/10.3390/s8084961

23. Liu J, Qiu L, Gao J, Jin Y (2006) Preparation, characterization and in vivo evaluation of formulation of baicalein with hydroxypropyl-β-cyclodextrin. Int J Pharm 312:137–143. https://doi.org/10.1016/j.ijpharm.2006.01.011

24. Hamdani U, Abbo H, Shaheeb E, Titinchi S (2019) Symmetrical and asymmetrical liquid crystal dimers: synthesis, characterisation and mesomorphic behaviour. Liq Cry 46(15):2291–2300. https://doi.org/10.1080/02678292.2019.1626925

25. Thadathil DA, Varghese S, Akshaya KB, Thomas R, Varghese A (2019) An insight into photophysical investigation of (E)-2-Fluoro-N'-(1-(4-Nitrophenyl) ethylidene) benzohydrazide through solvatochromism approaches and computational studies. J Fluorescence 29(4):1013–1027. https://doi.org/10.1007/s10895-019-02415-y

26. Kumari R, Varghese A, George L (2017) Estimation of ground-state and singlet excited-state dipole moments of substituted schiff bases containing oxazolidin-2-one moiety through solvatochromic methods. J Fluorescence 27(1):151–165. https://doi.org/10.1007/s10895-016-1942-9

27. Akshaya KB, Varghese A, Sudhakar YN, Lobo PL, George L (2017) Study on photophysical properties of N-arylphthalamic acid derivative containing 1, 2, 4-triazole scaffold. J Fluorescence 27(5):1909–1922. https://doi.org/10.1007/s10895-017-2129-8

28. Benesi HA, Hildebrand JHJ (1949) A spectrophotometric investigation of the interaction of iodine with aromatic hydrocarbons. J Am Chem Soc 71:2703–2707. https://doi.org/10.1021/ja01176a030

29. Maniyazagan M, Mohandoss S, Sivakumar K, Stalin T (2014) N-phenyl-1 naphthylamine/β cyclodextrin inclusion complex as a new fluorescent probe for rapid and visual detection of Pd2+. Spectrochim Acta A Mol Biomol Spectrosc 133:73–79. https://doi.org/10.1016/j.saa.2014.04.183

30. Sivakumar K, Ragi TR (2016) 2H1NA/β-cyclodextrin inclusion complex: Preparation, characterization and chemosensory application for detecting Ag+. J Macromol Sci A 53:677–686. https://doi.org/10.1080/10601325.2016.1224625

31. Salvatierra D, Díez C, Jaime C (1997) Host/guest interactions and NMR spectroscopy. A computer program for association constant determination. J Incl Phenom Mol Recognit Chem 27:215–231. https://doi.org/10.1023/A:1007989131909

32. Schneider HJ, Hacket F, Rudiger V, Iked H (1998) NMR studies of cyclodextrins and cyclodextrin complexes. Chem Rev 98:1755–1785. https://www.cheric.org/research/tech/periodicals/doi.php?art_seq=57241

33. Butkus E, Martins JC, Berg U (1996) 1 H NMR spectroscopic study of the interaction between cyclodextrins and bicyclo [3.3. 1] nonanes. J Incl Phenom Mol Recognit Chem 26:209–218. https://doi.org/10.1007/BF01053539

34. Dufour G, Evrard B, De Tullio P (2015) Rapid quantification of 2-hydroxypropyl-β-cyclodextrin in liquid pharmaceutical formulations by 1H nuclear magnetic resonance spectroscopy. Eur J Pharm Sci 73:20–28. https://doi.org/10.1016/j.ejps.2015.03.005

35. Desai C, Prabhakar B (2015) Nano-amorphous composites of cilostazol–HP-β-CD inclusion complexes: Physicochemical characterization, structure elucidation, thermodynamic studies and in vitro evaluation. J Incl Phenom Macrocycl Chem 81:175–191. https://doi.org/10.1007/s10847-014-0447-x

36. Liu M, Cao W, Sun Y, He Z (2014) Preparation, characterization and in vivo evaluation of formulation of repaglinide with hydroxypropyl-beta-cyclodextrin. Int J Pharm 477:159–166. https://doi.org/10.1016/j.ijpharm.2014.10.038

37. Zhang JQ, Wu D, Jiang KM, Zhang D, Zheng X et al (2015) Preparation, spectroscopy and molecular modelling studies of the inclusion complex of cordycepin with cyclodextrins. Carbohydr Res 406:55–64. https://doi.org/10.1016/j.carres.2015.01.005

38. Berg U, Bladh N, Hjelmencrantz A (2001) Structure and dynamic stability of cyclodextrin inclusion complexes with 1,4-disubstituted bicyclo[2.2.2]octanes. J Chem Soc Perkin Trans I 2:1850–1857. https://doi.org/10.1039/B100136L

39. Ren Z, Xu Y, Lu Z, Wang Z, Chen C, Guo Y et al (2019) Construction of a water-soluble and photostable rubropunctatin/β-cyclodextrin drug carrier. RSC Adv 9:11396–11405. https://doi.org/10.1039/C9RA00379G

40. Fan G, Zhang L, Shen Y, Shu G, Yuan Z, Lin J et al (2019) Comparative muscle irritation and pharmacokinetics of florfenicol-hydroxypropyl-β-cyclodextrin inclusion complex freeze-dried powder injection and florfenicol commercial injection in beagle dogs. Sci Rep 9:1–9. https://doi.org/10.1038/s41598-019-53304-0

41. Shervedani RK, Babadi MK (2006) Application of 2-mercaptobenzothiazole self-assembled monolayer on polycrystalline gold electrode as a nanosensor for determination of Ag (I). Talanta 69:741–746. https://doi.org/10.1016/j.talanta.2005.11.009

42. Saha RK (2016) Spectrophotometric micro determination of silver (I) using meloxicam as a new analytical reagent. Orient J Chem 32:499–507. https://doi.org/10.13005/ojc/320157

43. Abbasi S, Barzegaramiri H, Farmany A (2014) Determination of trace amounts of silver (I) in the presence of an activator with a kinetic method. Rare Met 33:731–736. https://doi.org/10.1007/s12598-014-0234-2

44. Kang YJ (2011) Copper and homocysteine in cardiovascular diseases. Pharmacol Ther 129:321–331. https://doi.org/10.1016/j.pharmthera.2010.11.004